Tellus (1990), *42A*, 259–269

Frontogenesis near steep orography

By G. HARTJENSTEIN and J. EGGER, *Meteorologisches Institut, Universität München, 8000 München 2, FRG*

(Manuscript received 8 July 1988; in final form 20 February 1989)

ABSTRACT

Fronts moving along steep mountain ridges may show the characteristics of a ducted gravity current. Moreover, an intensification of the cross-frontal temperature gradient and a sudden increase of the speed of propagation has been observed during the formation of such a ducted front. We propose a mechanism for this type of frontogenesis and demonstrate its effectivity by running numerical experiments with a multi-layer model.

1. Introduction

It is generally accepted that the flow along cold fronts is in approximate geostrophic balance with the mass field (e.g., Eliassen, 1962; Hoskins and Bretherton, 1972). However, if a cold front propagates parallel to a mountain barrier the along-front flow of cold air is blocked by the mountain below crest height. Geostrophic balance cannot be maintained and a current of cold air may protrude along the mountain which exhibits many characteristics of a ducted density current (Baines, 1980). The corresponding acceleration of the cold front near mountains is frequently observed in Australia (Coulman et al., 1985; Colquhoun et al., 1985), at the Appalachians (Bosart et al., 1973) and occurs also at the Pyrenees (Hoinka and Heimann, 1988) and the Alps (Heimann and Volkert, 1988). Although Garratt (1986) has shown that the land–sea contrast with its related differences in boundary-layer structure and heating rates has a strong impact on the acceleration and the deformation of fronts near the coastal mountains in south-east Australia these factors will be of no importance at many other mountain ranges.

There are indications that this acceleration of fronts near mountains is associated with frontogenesis. E.g., Coulman et al. (1985) note an increase of the cross-frontal temperature difference while fronts move along the coastal mountains of New South Wales. This increase can only be partially explained by the movement of the fronts into warmer regions and by differential diurnal heating of the post- and prefrontal air. Strong frontogenesis is also reported by Heimann and Volkert (1988) in their case study of frontal motion along the Alps (see also Fig. 12 and the related comments in the last section of this paper).

In this paper, we propose an explanation for this frontogenetic effect which is linked to the dynamics of stably stratified density currents. Egger and Haderlein (1987) (hereafter referred to as EH) have shown that blocking of along-front flow by mountains and the ensuing formation of ducted gravity currents at the mountain barrier ("orographic jet") can be simulated by aid of a simple one-layer model where the cold air is homogeneous. Frontogenesis is excluded in such a model a priori. We wish to demonstrate that frontogenesis at mountain ranges is almost inevitable in the situation considered by EH if the cold air is stably stratified. A multi-layer model is needed to study this problem.

2. The model

We use the isentropic coordinate model designed by Bleck (1984). The equations governing the model atmosphere are as follows. We assume hydrostatic adiabatic motion

$$d\theta/dt = 0, \quad (1)$$

so that the use of isentropic coordinates is feasible. The momentum equations are (f-plane)

$$\frac{\partial \boldsymbol{V}_{\mathrm{h}}}{\partial t}+\boldsymbol{V}_{\mathrm{h}} \cdot \nabla_\theta \boldsymbol{V}_{\mathrm{h}}+f \boldsymbol{k} \times \nabla_\theta \boldsymbol{V}_{\mathrm{h}}=-\nabla_\theta M-D \qquad (2)$$

where M is the Montgomery potential. As in Bleck (1974), the dissipative term D in (2) relies on the concept of eddy diffusion where the coefficient of diffusivity is proportional to the large-scale deformation. The continuity equation is

$$\frac{\partial}{\partial t}\left(\frac{\partial p}{\partial \theta}\right)+\nabla_\theta \cdot\left(\boldsymbol{V}_{\mathrm{h}} \frac{\partial p}{\partial \theta}\right)=0, \qquad (3)$$

where standard notation is used. The hydrostatic balance is

$$\frac{\partial M}{\partial \theta}=\Pi \qquad (4)$$

with the Exner function

$$\Pi=c_p\left(\frac{p}{p_0}\right)^{R/c_p}.$$

The numerical structure of the model is described to some detail in Bleck (1984). In the vertical, we have K isentropic layers ($K \geqslant 2$) with potential temperature θ_k, $1 \leqslant k \leqslant K$. The Montgomery potential M_k and the velocity $\boldsymbol{V}_k$ are defined within each layer, whereas the pressure p_k is defined at the interfaces between the layers. In particular, p_1 is surface pressure, $p_{K+1}=0$. The thickness of each layer is $\Delta p_k=p_k-p_{k+1}$.

The flow domain is a channel (width $B=$ 1400 km) with vertical walls as northern and southern boundaries. As in EH these walls represent steep mountain slopes. We use cyclic boundary conditions in zonal direction. Initially we assume a north–south orientated ridge of cold air in the channel (see Fig. 1).

In the two-layer model ($K=2$), the cold air is represented by the lower layer ($k=1$) while the interface of both layers is thought to represent the front. In particular, the surface front is located where this interface intersects the ground. In what follows, we shall refer to the two-layer model as the DISC-model since the front is represented by a discontinuity. The initial state can be characterized by the half width L_x of the cold air and by the values $\tilde{\Pi}_1(\tilde{p}_1)$, $\tilde{\Pi}_2(\tilde{p}_2)$ of the Exner function (pressure) at the axis of the cold air ridge which has a prescribed shape. Outside the cold air domain, the surface pressure is $p_1=p_2=p_0=1000$ hPa where the index 0 marks surface pressure values of the warm air, so that $\Pi_0=c_p$, in particular.

If $K>2$ (FTZ-model), a frontal transition zone (FTZ) is prescribed initially where the layers $1<k<K$ are densely packed while the first layer still represents the bulk of the cold air and the layer $k=K$ stands for the warm air above (Fig. 2). The initial surface Exner function Π_1 in the cold air domain is calculated prescribing a vanishing horizontal gradient of the Montgomery potential in the warm air ($k=K$)

$$\Pi_1=\frac{1}{\theta_1}\left(\Pi_0 \theta_K-\sum_{k=2}^{K} \Pi_k(\theta_k-\theta_{k-1})\right). \qquad (5)$$

The initial wind field is assumed to be in geostrophic balance so that we have northerly flow in the eastern part of the channel and southerly flow in the western part. For reasons of

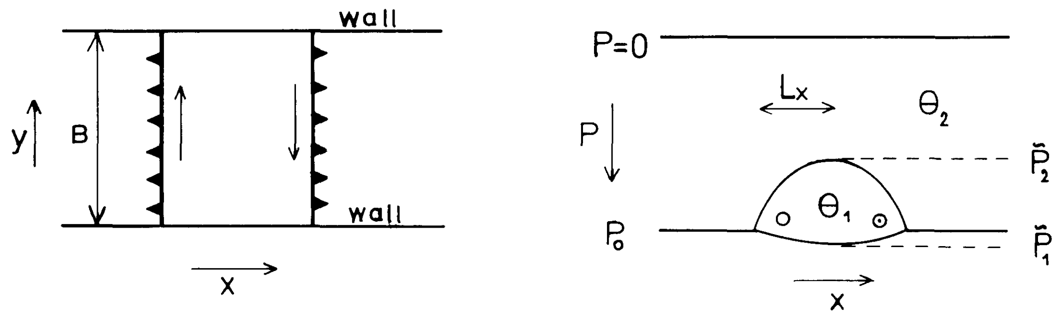

Fig. 1. Initial state in DISC-model (two-layer model) experiments. Left: Position of cold fronts and direction of geostrophic winds in the cold air mass. Right: Vertical cross-section showing the layers and interfaces.

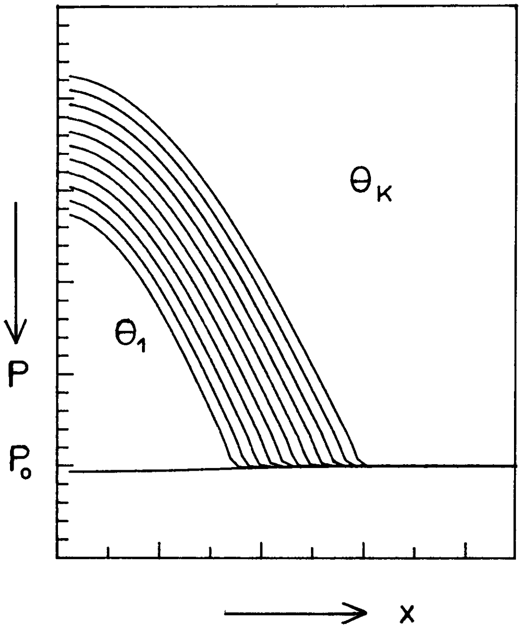

Fig. 2. Schematic figure of a FTZ (Frontal transition zone). Interfaces separating the cold air layer with $\theta = \theta_1$ from the warm air layer with $\theta = \theta_K$ are shown for the eastern part of the ridge of cold air.

symmetry it is sufficient to present results for the southern part of the channel.

We shall also employ a two-dimensional version of Bleck's model where there is no dependence of the flow on y and $f = 0$. This model can be used to simulate two-dimensional density currents in a nonrotating system. Since ducted currents at a wall behave to some extent like density currents in a nonrotating system we will use this economic two-dimensional model to explore some aspects of the propagation of density currents along a wall.

The horizontal grid size is $\Delta x = \Delta y = 100$ (25) km in the 3D-model (2D-model) which requires a time step of 100 (25) s.

3. Frontal propagation in the DISC-model

In this section, we use the DISC-model to recover and to refine some of the results obtained by EH. Of course, frontogenesis cannot occur in the two-layer model. However, DISC-model experiments on the propagation of the front at the southern wall will prove helpful to an understanding of the cases of frontogenesis presented later on.

We begin by presenting the flow evolution for a case with $L_x = 700$ km, $\tilde{p}_2 = 800$ hPa, $\theta_1 = 295$°K, $\theta_2 = 300$°K. The cold air has a cosine-profile initially. Fig. 3a shows the wind field in the lower layer and Fig. 3b the profile of the front at the wall at $t = 24$ h. The surface front protrudes rapidly towards the east at the southern wall of the channel and an orographic jet forms. Our results resemble those obtained by EH although EH used a one-layer model. EH demonstrated that the speed c of the density current at the wall can be estimated with good accuracy if the initial maximum depth H of the cold air is known: $c = \gamma(g'H)^{1/2}$, where $g' = g(\theta_2 - \theta_1)/\theta_2$ is a reduced gravity and $\gamma \sim 1$. We wish to test the applicability of this formula to the flow in the DISC-model, where $g'H$ must be replaced by the maximum initial deviation M_1' of the Montgomery potential within the cold air. Since $M_1 = \Pi_0 \theta_1$ at the surface front and $M_1 = \tilde{\Pi}_1 \theta_1$ at the axis of the cold air ridge ($\tilde{\Pi}_1$ follows from (5) with $K = 2$ and $\Pi_2 = \tilde{\Pi}_2$), we have

$$M_1' = \theta_1(\tilde{\Pi}_1 - \Pi_0), \tag{6}$$

and we expect in analogy to the conventional gravity current formula

$$c = \gamma(M_1')^{1/2}. \tag{7}$$

We test (7) by running the DISC-model using the same initial state as in the basic experiment shown in Fig. 3 except that we vary the difference $\theta_2 - \theta_1$. We identify c in (7) with the mean speed $\bar{c}$ of the current's nose in a 24 h integration of the model. The result is displayed in Fig. 4. Indeed, $\bar{c}$ and $(M_1')^{1/2}$ are linearly related with $\gamma = 0.85$, in good agreement with EH. However, (7) does not yield a perfect fit. Fig. 4 suggests

$$c = \gamma(M_1')^{1/2} - \varepsilon, \tag{8}$$

with $\varepsilon \approx 3$ m s^{-1}. Moreover, the current's speed is slightly reduced if we repeat the experiments but increase $\tilde{p}_2$ to 500 hPa (triangles in Fig. 4).

As has been pointed out above, the dynamics of trapped currents are similar to those of density currents in nonrotating systems. In particular, (8) applies to the latter case as well. We have repeated all experiments by running the two-

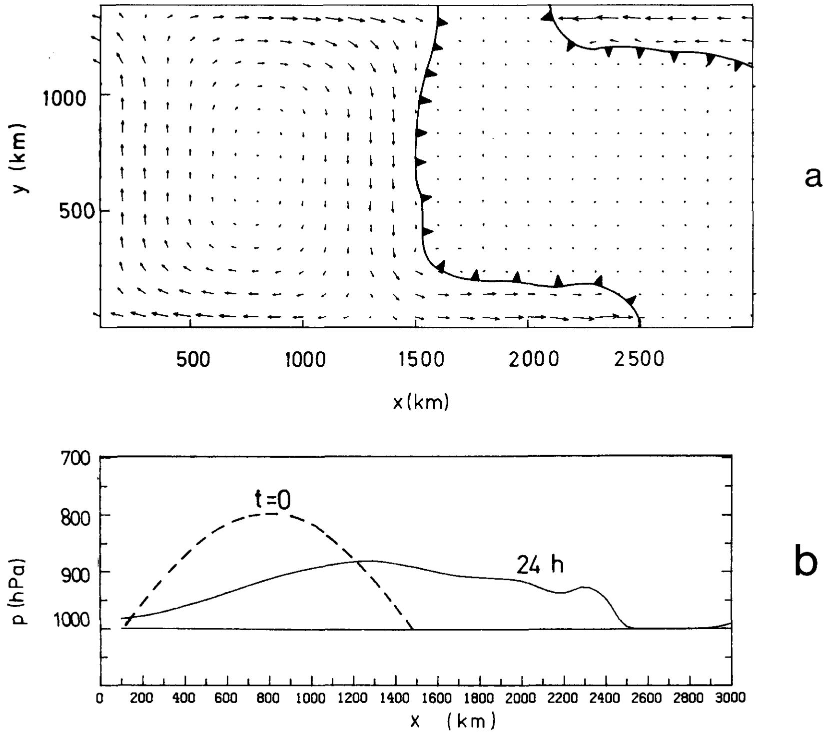

Fig. 3. DISC-model: 24 h forecast: (a) wind field in the cold air mass (maximum vector length is 14.3 m s^{-1}), (b) interface of the two layers at the southern wall (dashed: profile at $t = 0$).

dimensional version of the DISC-model (dashed line and circles in Fig. 4) to find that (8) fits the data very well for $\gamma = 0.74$. The speed of the nonrotating two-dimensional gravity current is slightly less than that of the corresponding trapped density current which is supported by mass flux towards the wall. Fig. 4 suggests that the propagation of trapped density currents at the wall can be studied by aid of a two-dimensional model. Since such a model is more economic the following experiments on the rôle of the additive "constant" ε in (8) are carried out by aid of the two-dimensional model. We test the hypotheses that ε may be linked to the total mass of the cold air or that ε is influenced by the initial slope of the front. Correspondingly we run experiments where the impact of variations of these factors can be seen. We list in Fig. 5 the mean speeds $\bar{c}$ as obtained for the various profiles shown. Note that M_1' has the same value in all three cases. We learn from an intercomparison of cases *a* and *b* that the total mass of the cold air has little impact at least during the first 24 h. However, the current appears to move faster the steeper the slope. The evolution of c in time is shown in Fig. 6 for cases (b) and (c). The currents need some time until they attain the full speed c_0 which is the same in both cases. However they differ in their initial acceleration which is greater the steeper the frontal slope. The last term in (8) is needed to capture this effect. We expect that (8) with $\varepsilon = 0$ yields a good fit if c is replaced by c_0. This expectation is confirmed by Fig. 7 where we show $\bar{c}$ and c_0 as a function of $(M_1')^{1/2}$ for cases (b) and (c).

However, there is a numerical problem with the determination of the speed c. The speed of propagation of surface fronts is sensitive to the specification of the flow variables in the layer of vanishing depth ahead of the surface front. As outlined in the Appendix the results shown in Figs. 4–7 are based on the reasonable assumption

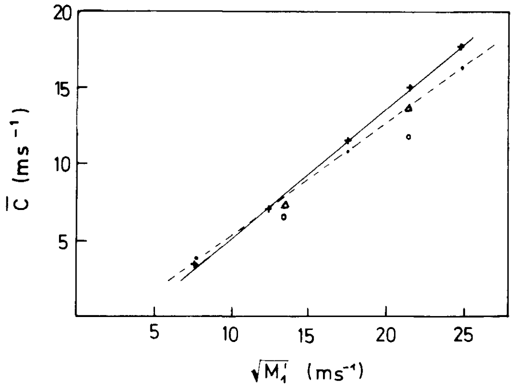

Fig. 4. Mean propagation speed of the front as a function of the densimetric velocity in the DISC-model. Full line: 3D model, $\tilde{p}_2 = 800$ hPa (triangles: $\tilde{p}_2 = 500$ hPa), dashed line: 2D model, $\tilde{p}_2 = 800$ hPa (circles: $\tilde{p}_2 = 500$ hPa). (The symbol ~ marks pressure values at the center of the cold air ridge.)

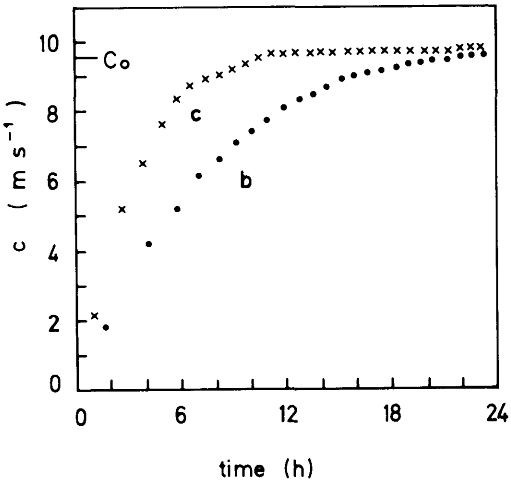

Fig. 6. Propagation speed as function of time for the profiles (b) and (c) of Fig. 5.

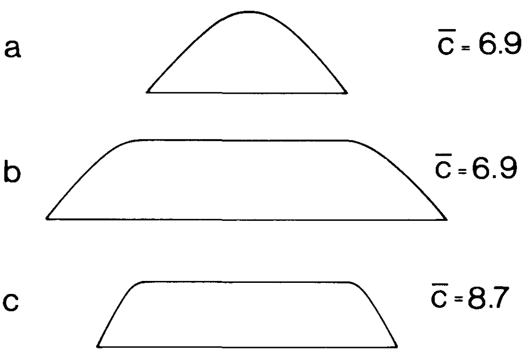

Fig. 5. DISC-model: Impact of the initial profiles of the cold air ridge on the mean speed $\bar{c}$ (m s^{-1}) of the first 24 h.

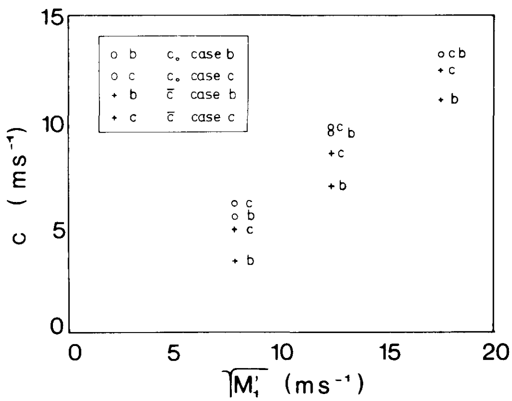

Fig. 7. Mean propagation speed ($\bar{c}$) and final propagation speed (c_0) for the profiles (b) and (c) of Fig. 5.

of vanishing flow speeds ahead of the front. However, somewhat different results are obtained if non-vanishing speeds are assumed (see Appendix).

We conclude that (8) gives a good fit but ε depends on the initial steepness of the front and, of course, on the averaging interval (24 h in our case). The steeper the front initially the smaller ε and the faster the steady state speed c_0 is attained. These results are to be contrasted to the steady state theory of two-dimensional gravity currents (e.g., Benjamin, 1968), where c is linearly related to $(g'h)^{1/2}$, h being the depth of the cold fluid behind the head. Here we study the initial stage of the flow evolution at the walls. This led us to introduce the initial value M_1' in (7).

4. Frontogenesis at mountain walls

Let us now consider the formation of a ducted gravity current in the presence of a frontal zone. We repeat the basic three-dimensional experiment but admit now three layers ($K = 3$) so that the frontal zone is represented by one layer of potential temperature $\theta_2 = 295°K$. We choose $\theta_1 = 290°K$, $\theta_3 = 300°K$, so that $\Delta\theta_1 = \theta_2 - \theta_1 = \Delta\theta_2 = \theta_3 - \theta_2 = 5°K$. Let us denote the position of the intersection of the first (second) interface with the ground by F_1 (F_2). We have $F_2 - F_1 = 200$ km initially. It is convenient to assess the strength of the frontal zone by the "gradient" $P = (\theta_3 - \theta_1)/(F_2 - F_1)$. Here we have $P = 0.5 \times 10^{-4}$ K m^{-1} initially.

After 24 h, we obtain again an intense density current at the southern wall. In Fig. 8a, we show the time evolution of the height profiles of both interfaces at the southern wall. Obviously F_1 moves much faster than F_2 and there is no transition zone near the ground at $t = 12$ h so that $P = \infty$. This is clearly a frontogenetic process. At $t = 24$ h, both interfaces coincide up to the depth of the coldest air. Of course, the frontogenetic process is strongly dependent on the choice of $\Delta\theta_1$ and $\Delta\theta_2$. If we choose $\Delta\theta_1 = 10°K$, $\Delta\theta_2 = 5°K$, F_1 catches up to F_2 within 6 h, whereas the frontogenetic process is fairly weak if $\Delta\theta_1 = 1°K$ (Fig. 8b and c).

To explain the frontogenesis near the wall we draw on the experience gained with the DISC-model. Let us assume that we have initially a multi-layer frontal transition zone (FTZ) as seen in Fig. 2. The FTZ can be characterized by the minimum values $\tilde{p}_k(\tilde{\Pi}_k)$ of the pressure (Exner function) in each layer. We can derive the deviation Montgomery potential M'_k for each layer by integrating the hydrostatic equation in the vertical. The integration starts with M'_1 defined through (6) where $\tilde{\Pi}_1$ is inserted from (5),

$$M'_1 = \Pi_0(\theta_K - \theta_1) - \sum_{k=2}^{K} \tilde{\Pi}_k(\theta_k - \theta_{k-1}), \tag{9}$$

and we find

$$M'_k = M'_{k-1} + (\theta_k - \theta_{k-1})(\tilde{\Pi}_k - \Pi_0), \quad 2 \leqslant k \leqslant K. \tag{10}$$

Since $\theta_{k-1} < \theta_k$, $\tilde{\Pi}_k < \Pi_0$, it follows

$$M'_{k-1} > M'_k. \tag{11}$$

We suggest that the speed c_k of the intersection F_k of an interface with the ground can be determined in agreement with what has been found for the DISC-model. Initially, c_k depends to some extent on the initial slope of the interface near the ground but we expect

$$c_k = \gamma_k (M'_k)^{1/2} \tag{12}$$

after some time. Thus, if

$$\gamma_k/\gamma_{k-1} < (M'_{k-1}/M'_k)^{1/2}, \tag{13}$$

it follows from (11)

$$c_{k-1} > c_k, \tag{14}$$

which means frontogenesis near the surface. The condition (13) for frontogenetic behaviour is certainly satisfied if $\gamma_k/\gamma_{k-1} \approx 1$, which seems to be an acceptable estimate.

The experiments displayed in Fig. 8 corroborate this simple conjecture. An extensive testing of this conjecture in parameter space with the three-dimensional model is prohibitive. In what follows, we report on further experiments on the frontogenetic process in the two-dimensional model.

We conduct a series of experiments with a FTZ consisting of 10 layers ($K = 12$). We choose $\Delta\theta_k = 0.5°K$ (Fig. 9a) so that the total temperature difference across the FTZ is 5.5°K. The width $F_{11} - F_1$ is 250 km initially. As predicted by (14), F_1 moves fastest and after 12 h all interfaces have merged. We modify now our initial state to test our basic concept. First we increase the width of the frontal zone (Fig. 9b). We expect that the merging will be slowed down. Indeed, we observe again frontogenesis but $F_{11} - F_1$ is still finite after 12 h. Next we decrease $\Delta\theta_k$ to 0.1°K (Fig. 9c). This reduces c_k considerably. Frontogenesis will be rather weak in such a case as is observed indeed. If we increase the steepness of the front the initial speeds c_k are increased and we obtain a more rapid merging of the interfaces (Fig. 9d). We can also impose a variation of $\Delta F_k \equiv F_k - F_{k-1}$ (i.e., a variation of the horizontal temperature gradient) within the FTZ. If ΔF_k increases with x (Fig. 9e) frontogenesis is much more rapid than if ΔF_k decreases (Fig. 9f). From these experiments we may conclude that frontogenesis in frontal zones at mountains can indeed be understood along the lines presented above.

It is of interest to compare the speed of the front in the DISC-model to that of the FTZ. To make the intercomparison meaningful we have to ensure that the arithmetic mean of all $\tilde{p}_k(\bar{p})$ is the same as $\tilde{p}_2$ in the DISC-model. Moreover the

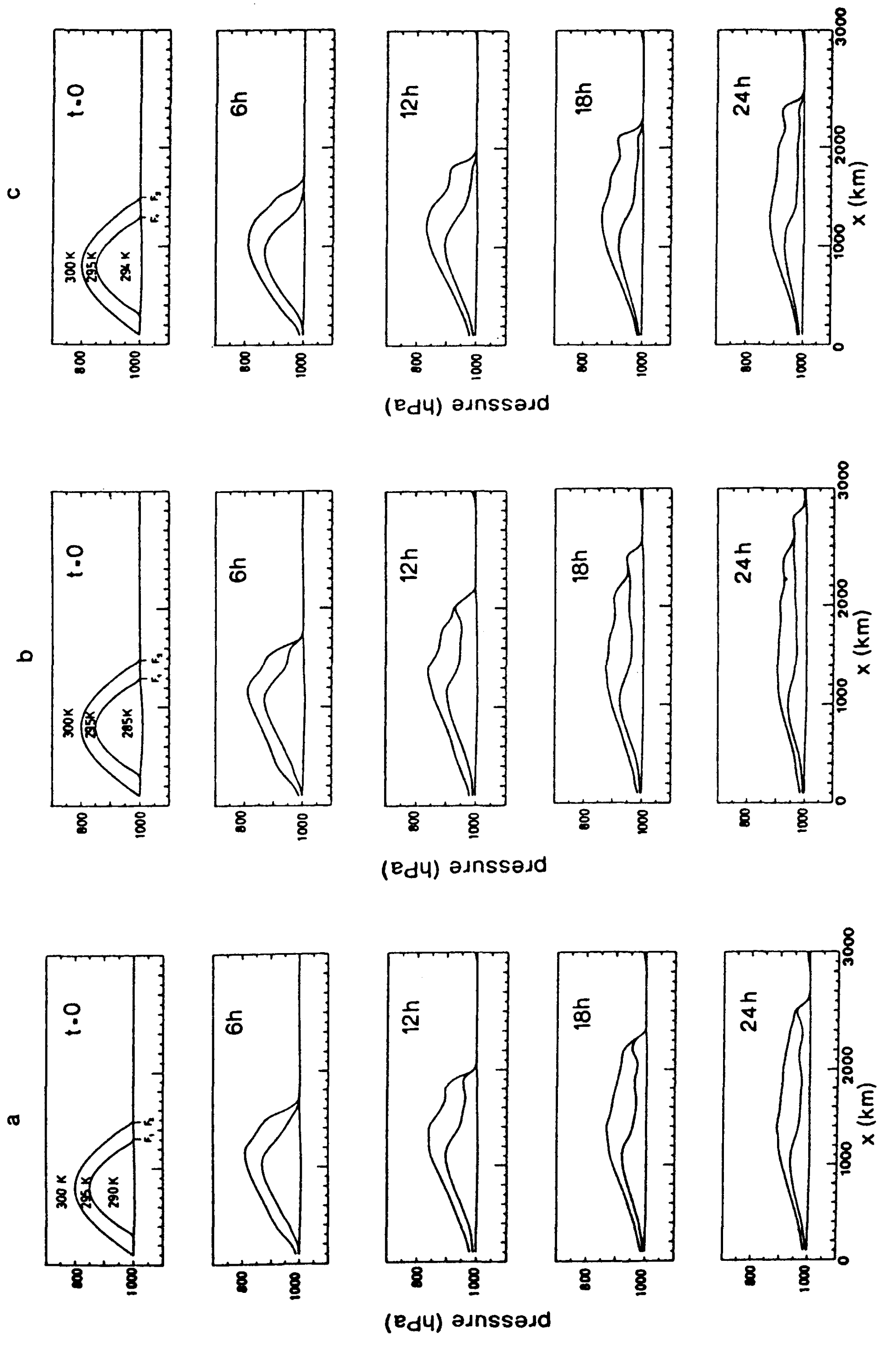

Fig. 8. Three-dimensional three-layer model: Time evolution of the interfaces at the southern wall. (a) $\Delta\theta_1 = \Delta\theta_2$, (b) $\Delta\theta_1 > \Delta\theta_2$, (c) $\Delta\theta_1 < \Delta\theta_2$.

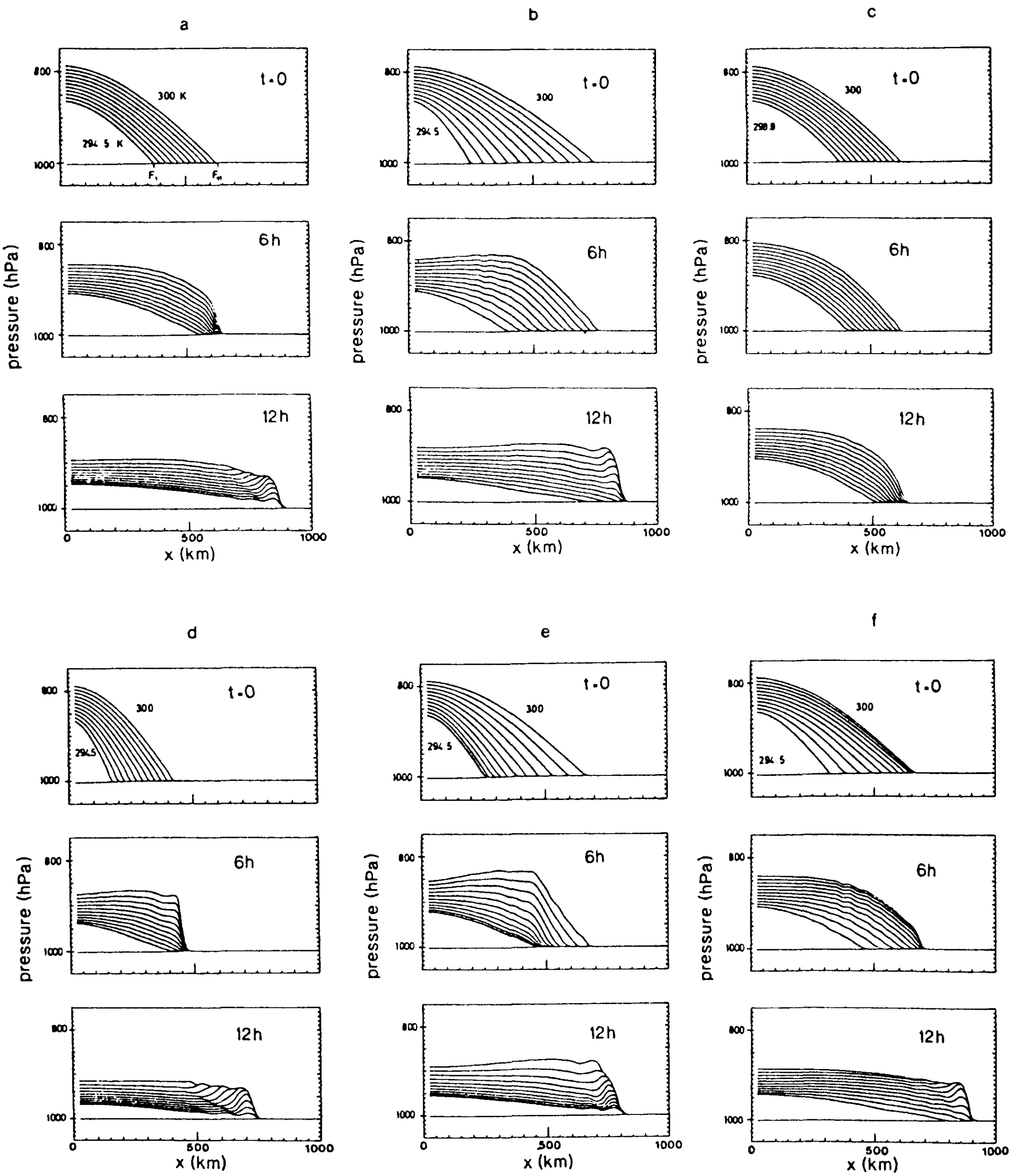

Fig. 9. 2D-model: Motion of the interfaces of FTZ's which differ from the reference case (a) by a smaller temperature gradient (b), smaller overall temperature contrast (c), steeper FTZ (d), horizontally varying temperature gradient (e and f).

overall temperature difference and the diameter of the cold air ridge must be the same in both models. Under these conditions M_1' in the FTZ-model attains the same value as M_1' in the DISC-model. We intercompare the speed c of the front in the DISC-model with the speed c_{11} in the FTZ-model. Of course propagation depends on how the position of the front is defined in the

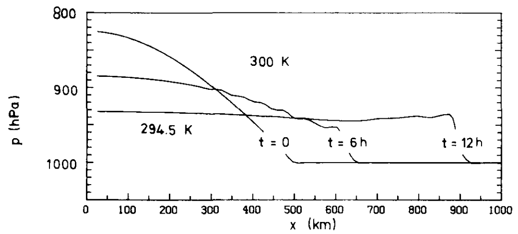

Fig. 10. Same as Fig. 9a, but for the DISC-model.

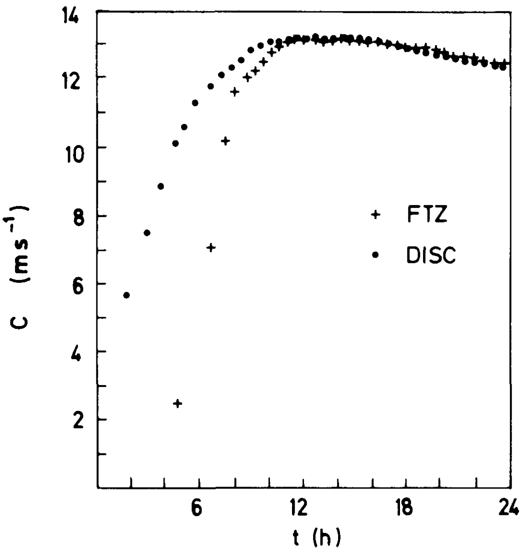

Fig. 11. Propagation speed as function of time. Comparison of the DISC-model and the FTZ-model.

case of the FTZ where initially the temperature gradient within the FTZ is independent of x. We choose F_{11} as the position of the front because here the temperature begins to drop and the maximum surface temperature gradient will develop just at this point when the gravity current begins to form. Fig. 10 shows the DISC-model run which compares to the FTZ-model run from Fig. 9a. We find that the time averaged propagation velocity is reduced by the frontogenetic process. Note, however, that there is almost no propagation during the first few hours and thereafter a drastic increase of propagation speed as can be extracted from Fig. 11, where we plot $c(t)$ for both model runs. Moreover we infer from Fig. 11 that after frontogenesis is over both gravity currents propagate with the same speed. Thus, (7) also applies to the FTZ-model, if c is considered as the propagation speed after the frontogenetic process is completed. Extensive testing gives $\gamma = 0.76$ for the FTZ-model in good agreement to the results for the DISC-model (see also Figs. 4, 7).

5. Discussion

So far we have demonstrated that frontogenesis must be expected whenever a frontal zone moves along a mountain barrier. The frontogenetic process is restricted to a relatively narrow belt to the north of the mountain wall (if an eastward moving front is considered). Concerning the acceleration of the front near the mountain wall we have to distinguish between the two models: in the DISC-model the front moves faster (compared to the original front) near the mountains (orographic jet). On the other hand, if we consider a frontal zone (FTZ-model) the formation of the orographic jet is first delayed as a consequence of frontogenesis, and after frontogenesis has stopped a drastic acceleration of the frontal nose results.

We have to stress that we have been looking at a highly idealized situation. For example, frontal propagation at mountains in actual cases is strongly influenced by flow conditions at larger scales while the front studied in our 3D-runs would be stationary if there were no wall at the boundary. Also, we did not allow for flow over the mountain. Nevertheless we expect that the frontogenetic process as described here is acting at the Alps, say, although it may prove difficult to separate it from other factors on the basis of case studies.

We propose that the rapid frontogenesis on 3 May 1987 can be interpreted as an example of the mechanism outlined in this paper. The formation and acceleration of this front which moved along the northern rim of the Alps is documented in Heimann and Volkert (1988). There are some indications that confluence at the head of an orographically ducted gravity current caused frontogenesis in that case: there is a distinct increase (with respect to time) of the cross-frontal temperature gradient near the Alps, whereas this feature is not observed further to the north. In

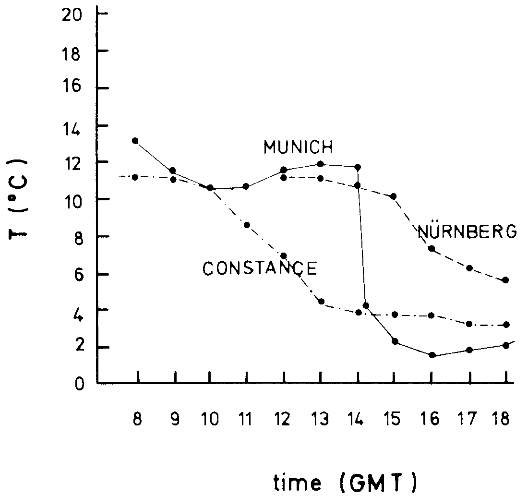

Fig. 12. Time variation of temperature during the passage of the May 3rd front at Constance, Munich, Nürnberg.

Fig. 12, we plot the decrease of temperature associated with the frontal passage at three different locations: Constance (about 180 km west of Munich), Munich and Nürnberg (about 150 km north of Munich). It is only in Munich that a drastic drop of the temperature is observed. According to Fig. 5 of Heimann and Volkert (1988) the speed of the front is about 50 km/h between Constance and Munich. After the front passed Munich a propagation speed of about 100 km/h is observed.* The temperature falls at a rate of 2°K/h in Constance (11 GMT) but of 8°K/0.5 h in Munich (14 GMT). Thus the temperature gradient across the front increases from 0.4°K/10 km to 3.2°K/10 km in 3 h (i.e., $2.6 \cdot 10^{-8}$ K m^{-1} s^{-1}). In contrast to Munich, we find at the same time a cross-frontal temperature gradient of only 1.2 °K/10 km in Nürnberg. These observations agree qualitatively with the model results presented in this paper. We propose that the drastic acceleration of the front is linked to this frontogenetic effect. Yet, there is an additional reason for a further acceleration of the front in this case: near Linz (200 km east of Munich), the cold air current caught up with a foregoing cold front which was nearly stationary. This resulted in an additional increase of the cross-frontal temperature contrast. Moreover, the model results obtained by Heimann (1988) suggest that cooling due to precipitation may have contributed to frontogenesis, too.

* In the paper of Heimann and Volkert the analysis of the front position is erroneous east of Munich. In fact, the front passed Salzburg (120 km east of Munich) between 1500 and 1520 GMT (Munich at about 14 GMT) so that the propagation speed nearly doubled.

6. Appendix

In a numerical experiment, we solve the momentum equations and the equation of continuity for an isentropic layer even at those grid points where the layer has vanishing depth. The Montgomery potential in such a point is set equal to the Montgomery potential of the first layer above which has nonvanishing depth. This implies that the velocities V_0 in the massless layers equal the velocities of the first nonvanishing layer. In particular, the velocities V_0 in the DISC-model vanish because the warm air mass is at rest initially and remains at rest at those grid points where the cold air mass has vanishing depth. The assumption of vanishing velocity in a layer of vanishing depth is certainly reasonable

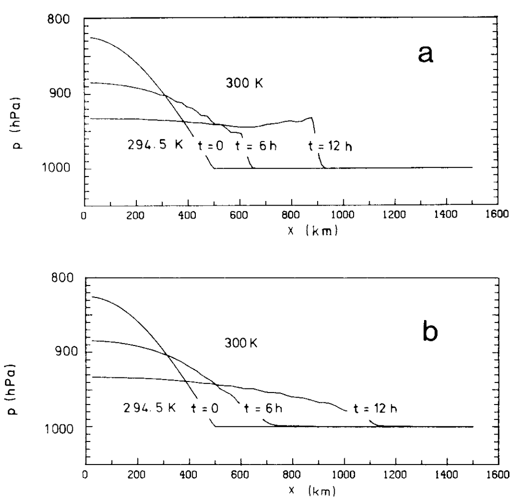

Fig. 13. 12-h run of the 2-dimensional DISC-model with (a) $U_0 = 0$ (which is the same as in Fig. 10) and (b) $U_0 = (M'_1)^{1/2}$.

but nevertheless somewhat arbitrary and, unfortunately, not without consequences since V_0 enters the finite difference approximation to the term $V_h \cdot \nabla_\theta V_h$ in (2) at the surface front. In turn, the speed of propagation of the front is influenced by the choice of V_0.

In Fig. 13, we compare a run with the 2-dimensional DISC-model where the zonal speed $U_0 = 0$ to a run where $U_0 = (M_1')^{1/2}$. It is evident that the height profile of the cold air mass is flatter and c is larger in the second experiment. Similar tests have been made for the FTZ-model. We found essentially the same effects as depicted in Fig. 13. However, the frontogenetic process is little affected by the choice of V_0.

REFERENCES

Baines, P. G. 1980. The dynamics of the southerly buster. *Austr. Met. Mag. 28*, 175–198.

Benjamin, J. B. 1968. Gravity currents and related phenomena. *J. Fluid Mech. 31*, 209–248.

Bosart, L. F., Pagnotti, V. and Lettau, B. 1973. Climatological aspects of Eastern United States back-door cold frontal passages. *Mon. Weath. Rev. 101*, 627–635.

Bleck, R. 1974. Short-range prediction in isentropic coordinates with filtered and unfiltered numerical models. *Mon. Weath. Rev. 102*, 813–829.

Bleck, R. 1984. An isentropic coordinate model suitable for lee cyclogenesis simulation. *Riv. Met. Aeronaut. 44*, 189–194.

Colquhoun, J. R., Shepherd, D. J., Coulman, C. E., Smith, R. K. and McInnes, K. 1985. The southerly burster of south eastern Australia: an orographically forced cold front. *Mon. Wea. Rev. 113*, 2090–2107.

Coulman, C. E., Colquhoun, J. R., Smith, R. K. and McInnes, K. 1985. Orographically-forced cold fronts—mean structure and motion. *Bound. Layer Met. 32*, 57–83.

Egger, J. and Haderlein, K. 1987. Fronts near orography in a one-layer model. Short- and Medium-Range Numerical Weather Prediction. *Proceedings from WMO/IUGG NWP Symposium*, Tokyo, August 1986, 757–766.

Eliassen, A. 1962. On the vertical circulation in frontal zones. *Geofys. Publikasjoner 24*, No. 4, 147–160.

Garratt, J. R. 1986. Boundary-layer effects on cold fronts at a coastline. *Bound. Layer Met. 36*, 101–105.

Heimann, D. and Volkert, H. 1988. The "Papal front" of 3 May 1987—mesoscale analyses of Routine Data. *Beitr. Phys. Atmosph. 61*, 62–68.

Heimann, D. 1988. The "Papal front" of 3 May 1987: Modelling of orographic and diabatic effects. *Beitr. Phys. Atmosph. 61*, 330–343.

Hoinka, K. P. and Heimann, D. 1988. Orographic channeling of a cold front at the Pyrenees. *Mon. Wea. Rev. 116*, 1817–1823.

Hoskins, B. J. and Bretherton, F. P. 1972. Atmospheric frontogenesis models: Mathematical formulation and solution. *J. Atmos. Sci. 29*, 11–37.